Inclusion of *A Priori* Information in Segmentation of Colon Lumen for 3D Virtual Colonoscopy[1)]

Z. Liang, F. Yang, M. Wax, J. Li, J. You, A. Kaufman, L. Hong, H. Li and A. Viswambharan

Departments of Radiology and Computer Science, State University of New York, Stony Brook, NY 11794

Abstract

Segmentation of colon lumen from computed tomography (CT) is necessary for 3D virtual colonoscopy. Identifying the residual fluid retained inside the colon after colon-cleansing procedure is one of the major tasks for the segmentation. This work developed a computer algorithm to segment out the residual fluid after the image intensity of the fluid has been enhanced by ingesting an adequate amount of contrasting solution of Diatrizoate Meglumine and Diatrizoate Sodium. The algorithm models the image-intensity statistics across the field-of-view (FOV) as a mixture of Gaussian functional and assumes a Markov random field (MRF) for the labels of the underline tissue distribution. The model parameters of the mixture are fitted to the image data by the maximum-likehood estimator. In the fitting, the *a priori* known attenuation coefficients of air (inside the colon), soft tissue (fat) and muscle are included as the initial estimate. As iteration progresses, the initial estimate is tuned to fit into the image data. The optimal number of tissue types is determined by an information criterion. With the determined number of tissue types and the fitted model parameters of the mixture, each image pixel is classified obeying the assumption of MRF across the FOV. The algorithm was tested by acquired CT abdomen images. Its performance was very encouraging. The computing efficiency was significantly improved when the histogram of the image data was used.

I. INTRODUCTION

Colon and rectum cancer has been the second leading cause of cancer deaths across this nation [10,12]. A cost-effective and patient-comfortable screening procedure is necessary to diagnose the disease at an earlier stage. We have been developing an innovative technology, called 3D virtual colonoscopy, for massive colon screening [3,4]. This technology uses a computer system to navigate through the colon model reconstructed from computed tomography (CT) data. It has been shown that this technology is effective in imaging colonic polyps as small as 3mm in diameter [5,14]. (It is known that polyps of size greater than 5mm in diameter will progress toward malignant carcinoma [9,13]). However, this technology requires that the colon is clean, free of fluid and stool inside. In clinic, it is almost impossible to distinguish the fluid and stool from the colon surface in the CT images.

1) This work was supported by Grant #HL54166 of the National Heart, Lung, and Blood Institute; Grant #NS53833 of the National Institute of Neurological Disorders and Stroke; Established Investigatorship of the American Heart Association; ITG Grant of the Center for Biotechnology of New York State and E-Z-EM Inc.

This work aims to use contrast agents to enhance the image intensity of the fluid and then apply computer algorithms to segment the fluid from the CT scans. A similar approach should be applicable to segment the stool.

II. METHODS

Following the colon-cleansing procedure of optical colonoscopy in which one gallon of Golytely solution is ingested by the patient during the day prior to the study, 120 ml solution of Diatrizoate Meglumine and Diatrizoate Sodium was mixed with the Golytely in order to enhance the fluid density for CT scans. After the colon was inflated by approximately 1000 cc air through the rectum, a CT scan was performed for the whole colon in a helical mode (1:1.7 pitch) with 120 kVp and 220 mA settings. (We have used variable protocols of 1:1.5 pitch to 1:2.0 pitch and 220 mA to 280 mA for several patients. No noticeable change of image quality was observed).

The body boundaries in the CT images were first detected by a computer program to eliminate the voxels outside the body for image-segmentation task. This step will save a significant computing time for image segmentation. The histogram of the body voxels was then computed. The histogram identifies the CT numbers of the known attenuation coefficients of air (inside the colon), soft tissue (fat) and muscle, see Fig.1. This figure shows a typical histogram from abdomen CT images. The three peaks corresponding to the air, soft tissue and muscle are well characterized by a Gaussian functional with different means and variances. Given the CT protocol setting of kVp, the means (or locations) of these three peaks are *a priori* known. With mA increases from 220 to 280, the peak width (or variance) varies slightly. The histogram was saved in the computer for later use in fitting the image data for tissue parameters.

The parameter estimation and segmentation algorithms [7,8] were developed to consider the CT image characteristics, see Appendix: (a) a single parametric (attenuation coefficient) image, different from the multispectral (T_1, T_2 and proton density) magnetic resonance (MR) images; (b) known attenuation coefficients of air, soft tissue and muscle; (c) a large dynamic range of the image intensity for bone beyond the muscle, including the enhanced fluid, see Fig.1, and (d) a flat range of intensity between the classes of air and soft tissue, due to partial volume effect. The histogram of Fig.1 contains all the above information and, therefore, should be used in fitting the data. The use of histogram saved a significant computing time. This is very important, since the segmentation should be in real time. Furthermore a routine CT scan generates up to 500 images of 512^2 size which

should be handled by a currently available computer power of moderate memory.

III. RESULTS

A typical slice image of 512^2 size and 5 mm thick is shown on the left of Fig.2. A horizontal profile (on the right) of one-pixel wide was drawn at the location as indicated on the image. The enhanced fluid is noticeable.

By the threshold of skin pixel value, we identified a boundary pixel on the y-axis by tracing along the axis from $+\infty$ toward $-\infty$ on the slice image of Fig.2. Then we searched among the nearby pixels of the identified one (along a radius relative to the image center) to find another boundary pixel following clockwise rotation. The pixels outside the boundary were stripped away. Figure 3 shows the found boundary (on the left) and the slice image after the stripping (on the right).

The above boundary search was applied to all 46 slices which covered the whole colon. The voxels outside the body were labeled as background and ignored since they do not contribute to the tissue segmentation. This step eliminates the extra computing time for the voxels outside the body.

All the voxels inside the body contour were considered to generate the histogram of Fig.1. From the histogram, initial estimates on the means were selected at the locations of the peak centers, respectively. The initial estimates on the variance and mixture weights were obtained by the peak width of FWHM (full-width-at-half-maximum) and the relative area of the peaks, respectively. We started by assuming only three classes defined by the three peaks (air, soft tissue and muscle). The parameter estimation algorithm of eqns.(8), (9), (11) and (12) as shown in the Appendix was applied. After the iterative algorithm converged to a stable solution, the modified MDL (minimum description length) information criterion was calculated [7]. Then we increased the number of classes by putting more new classes between the three peaks and beyond the muscle peak, until the information criterion reached the minimum (six classes). The initial means of the new classes were equally spaced between the peaks. Each initial variance and mixture weight were chosen as the average of two nearby peaks, respectively.

The table below lists the chosen initial estimate of the means (i.e., the CT numbers of the attenuation coefficients of the air, soft tissue and muscle) and the iterated results (the mixture weights, the means and the variances of the Gaussian functional) by the parameter-estimation algorithm.

For the case of three classes, the three initial means of 65, 905, 1060 were deviated away by those voxels of bone and enhanced fluid, as well as the partial volume voxels. In the case of six classes, the three initial means on the peaks were relatively preserved. The wide ranges of the partial volume voxels and of the bone and enhanced fluid were satisfactorily fitted by the other three new classes which had large variances. The six-class estimation gave the maximum-likelihood fit of the tissue parameters and best fit of the information criterion.

Chosen Initial Means and Estimated Parameters

classes	Initial	Weight	Mean	Variance
3	65.0	0.097	70.6	645.8
	905.0	0.770	963.5	5892.0
	1060.0	0.132	667.9	186800.0
6	65.0	0.094	68.2	552.2
	350.0	0.051	233.9	10250.0
	650.0	0.053	795.6	78090.0
	905.0	0.438	907.8	433.7
	1060.0	0.313	1042.0	1658.0
	1600.0	0.051	1037.0	112400.0

For comparison purpose, we segmented the CT image by thresholds of the initial estimates on the six classes. Class 1 covers voxel values from 0 to 75; class 2 from 76 to 130; class 3 from 131 to 830; class 4 from 831 to 980; class 5 from 981 to 1125; and class 6 has voxel value beyond 1125. These six classes are shown by Fig.4. By the MAP (maximum *a posteriori* probability) segmentation utilizing a MRF prior model of the Appendix, the segmented six classes are shown by Fig.5.

Figure 6 show the summation of the three segmented classes of the air, the lower part of the partial volumes on the histogram and the enhanced fluid, i.e., the summation of those segments two on the top and one in the bottom right of Fig.4 (left) and Fig.5 (right). The bone was also included in the segment summation. Since the bone is far away from the colon, so the inclusion will not affect the colon visualization. Figure 7 show the colon-cleansed CT images using the segmented colon lumen of Fig.6, respectively. It is noted that the boundary between the enhanced fluid and the air inside the colon was completely eliminated with the MAP segmentation (on the right). The boundary is a serious problem for threshold segmentation techniques (on the left). The fluid on the lower left of the MAP results was not segmented due to its similar characteristics as that of the muscle. Therefore, a higher contrast solution is suggested. The MAP segmented CT image has a clean colon lumen and retains original data inside the body boundary (voxels outside the body were stripped away). It is now available for the 3D virtual colonoscopy.

IV. CONCLUSIONS

A procedure for segmentation of contrast-enhanced fluid inside the colon was described. A MAP approach was compared to threshold segmentation and showed significant improvement on the removal of the boundary between the fluid and the air inside the colon. *A priori* information on the known attenuation coefficients of body tissues and the orientation of the fluid/air boundary was utilized. An efficient calculation of the tissue parameters was presented based on the histogram of single parametric images. The MAP approach should be applicable to the segmentation of the residual stool.

0-7803-4261-5/98/$10.00 (c) 1998 IEEE

V. APPENDIX

The likelihood for each pixel Y_{ij}, on an image array $\{1 \le i \le I,\ 1 \le j \le J\}$, falling into K classes is described by

$$g(Y_{ij} \mid W, \Theta) = \sum_{k=1}^{K} w_k \, p_k(Y_{ij} \mid \theta_k) \tag{1}$$

where $p_k(Y_{ij} \mid \theta_k)$ is the probability distribution of Y_{ij}, given θ_k, and w_k is the mixture weight which can depend on neighborhood [1,6]. There is $\sum_k w_k = 1$. $\Theta = \{\theta_k\}$ is the class parameters to be estimated. Assume all pixels are independent each other, the likelihood of observing $Y = \{Y_{ij}\}$ given the K classes is then expressed as

$$G(Y \mid W, \Theta) = \prod_{i=1,j=1}^{i=I,j=J} g(Y_{ij} \mid W, \Theta) . \tag{2}$$

The tracing on all pixels $\{i,j\}$ for the maximum-likelihood solution of W and Θ is time consuming and may not be necessary for a single parametric image, since many pixels may have nearly the same density value. The inclusion of histogram will greatly reduce the computing time [2,11].

Introducing an index $m = 1,2,...,M$ for the pixel value range $Y_{\min} \le Y_m \le Y_{\max}$, such that $Y_1 = Y_{\min}$ and $Y_M = Y_{\max}$, where M is large enough so that the discretizing of continuous variable Y will not introduce noticeable error. (By modern medical imagers with digital computers, the outputs are in discrete form. So the M is determined by the output). Let $H(m)$ be the histogram of the image data $\{Y_{ij}\}$. The likelihood of each datum Y_m (not pixel) falling into K classes is then given by

$$g(Y_m \mid W, \Theta) = \sum_{k=1}^{K} w_k \, p_k(Y_m \mid \theta_k) . \tag{3}$$

The likelihood for all pixels now becomes

$$G(Y \mid W, \Theta) = \prod_{m=1}^{M} [\, g(Y_m \mid W, \Theta) \,]^{H(m)} . \tag{4}$$

By the EM technique, each pixel (i,j) is completely specified by the true pixel value $\{X_{ij}\}$ and the indicator $Z_{k(i,j)}$ which indicates that pixel (i,j) is belong to class k. In terms of discrete histogram form, we have, for each datum X_m,

$$f(X_m \mid W, \Theta) = \prod_{k=1}^{K} w_k^{Z_{km}} \, p_k^{Z_{km}}(Y_m \mid \theta_k) \tag{5}$$

and for all independent data,

$$F(X \mid W, \Theta) = \prod_{m=1}^{M} [\, f(X_m \mid W, \Theta) \,]^{H(m)} . \tag{6}$$

The E-step of the EM technique can be expressed as

$$Q(\ln F \mid Y, W^{(n)}, \Theta^{(n)}) = \sum_m \left\{ \sum_k [\, Z_{km}^{(n)} \, H(m) \ln w_k + Z_{km}^{(n)} \, H(m) \ln p_k(Y_m \mid \theta_k) \,] \right\} \tag{7}$$

where

$$Z_{km}^{(n)} = E[Z_{km} \mid Y, W^{(n)}, \Theta^{(n)}) = \frac{w_k^{(n)} \, p_k(Y_m \mid \theta_k^{(n)})}{g(Y_m \mid W^{(n)}, \Theta^{(n)})} . \tag{8}$$

The M-step maximizes $Q(.)$ with respect to w_k and θ_k, respectively. Due to the condition of $\sum_k w_k = 1$, the M-step maximizes $Q(.) - \lambda (\sum_k w_k - 1)$ with respect to w_k,

$$w_k^{(n+1)} = \frac{1}{\lambda} \sum_m Z_{km}^{(n)} \, H(m) \tag{9}$$

where parameter $\lambda = \sum_m H(m) = N$ (the number of pixels inside the body contour). For Gaussian statistics

$$p_k(Y_m \mid \theta_k) = \frac{1}{\sqrt{2\pi \nu_k}} \, exp\,[\, -(Y_m - \mu_k)^2 / 2\nu_k] \tag{10}$$

where μ_k is the mean of pixel values in class k and ν_k is the variance, the maximization results are

$$\mu_k^{(n+1)} = \frac{\sum_m Z_{km}^{(n)} \, H(m) \, Y_m}{\sum_m Z_{km}^{(n)} \, H(m)} \tag{11}$$

and

$$\nu_k^{(n+1)} = \frac{\sum_m Z_{km}^{(n)} \, H(m) \, (Y_m - \mu_k^{(n+1)})^2}{\sum_m Z_{km}^{(n)} \, H(m)} . \tag{12}$$

A MRF prior is constructed to remove both isolated voxels and the boundary between the fluid and the air inside the colon. Mathematically it is written as

$$p(\Theta) = \alpha^{-1} exp\,[\, -U(\mathbf{l}) / \beta \,] \tag{13}$$

where α is a normalization constant and $\beta = 1.0$ was used [8]. The energy function is defined, in two dimensions, as

$$U(\mathbf{l}) = \sum_i \left\{ \sum_r [1 - \delta(l_i - l_r)] + \sum_s [1 - \delta(l_i - l_s)] / \sqrt{2} + \sum_t [1 - \delta(l_i - l_t)] / \sqrt{5} \right\} \tag{14}$$

where $\delta(0) = 1$, $\delta(\neq 0) = 0$ and $\{l_i\}$ are the pixel labels. The index r runs over the 4 first-order neighbors and s runs over the 4 second-order pixels. These two orders aim to remove the isolated pixels. In order to consider the *a priori* information about the (horizontal) orientation of the boundary between the fluid and the air inside the colon, we introduced the third index t which runs over the fourth-order neighbors. A similar description can be made in three dimensions for first-, second-, and fourth-order voxels.

VI. ACKNOWLEDGMENT

The authors appreciate Dr. Gene R. Gindi for his assistance in preparing this manuscript and Dr. Donald P. Harrington for his encouragement and valuable comments.

VII. REFERENCES

[1] S.S. Gopal and T.J. Hebert (1997), "Maximum Likelihood Pixel Labeling Using a Spatially-Variant Finite Mixture Model", IEEE Trans Nucl Sci **44**: 1578-1582.

[2] T.J. Hebert (1997), "Fast Iterative Segmentation of High Resolution Medical Images", IEEE Trans Nucl Sci **44**: 1362-1367.

[3] L. Hong, A. Kaufman, Y. Wei, A. Viswambharan, M. Wax and Z. Liang (1995), "3D Virtual Colonoscopy", *IEEE Biomedical Visualization Symposium*, IEEE CS Press, CA, 26-32.

[4] L. Hong, A. Kaufman, Z. Liang, A. Viswambharan and M. Wax (1996), "Visible Human Virtual Colonoscopy", Conference of National Library of Medicine Visible Human Project, pp.29-30.

[5] L. Hong, Z. Liang, A. Viswambharan, A. Kaufman and M. Wax (1997), "Reconstruction and Visualization of 3D Models of Colonic Surface", IEEE Trans Nucl Sci **44**: 1297-1302.

[6] Z. Liang, R. Jaszczak and R. Coleman (1991), "On Reconstruction and Segmentation of Piecewise Continuous Images", Proc IPMI, **12**: 94-104.

[7] Z. Liang, R. Jaszczak and R. Coleman (1992), "Parameter Estimation of Finite Mixtures Using the EM Algorithm and Information Criteria with Applications to Medical Image Processing", IEEE Trans Nucl Sci **39**: 1126-1133.

[8] Z. Liang, J. MacFall and D. Harrington (1994), "Parameter Estimation and Tissue Segmentation from Multispectral MR Images", IEEE Trans Med Imag **13**: 441-449.

[9] T. Muto, H. Bussey and B. Morson (1975), "The Evolution of Cancer of the Colon and Rectum", Cancer **36**: 2251-2270.

[10] M. O'Brien S. Winawer and A. Zauber (1990), "The National Polyp Study: Patient and polyp characteristics associated with high-grade dysplasia in colorectal adenomas", Gastroenterology **98**: 371-379.

[11] J. Peter, R. Freyer, M. Smith, C. Scarfone, R. Coleman and R. Jaszczak (1997), "Nuclear Medicine Image Segmentation Using a Connective Network", IEEE Trans Nucl Sc **44**: 1583-1590.

[12] J. Potter and M. Slattery (1993), "Colon Cancer: A review of the epidemiology", Epidemiol Rev **15**: 499-545.

[13] B. Simons, A. Morrison, R. Lev and W. Verhoek-Oftendahl (1992), "Relationship of Polyps to Cancer of the Large Intestine", J Natl Cancer Inst **84**: 962-966.

[14] A. Viswambharan, M. Wax, L. Hong, A. Kaufman and Z. Liang (1996), "Virtual Colonoscopy: 3D visualization of the mucosal surface of the colon", Annual Meeting of Radiological Society of North America, pp.565.

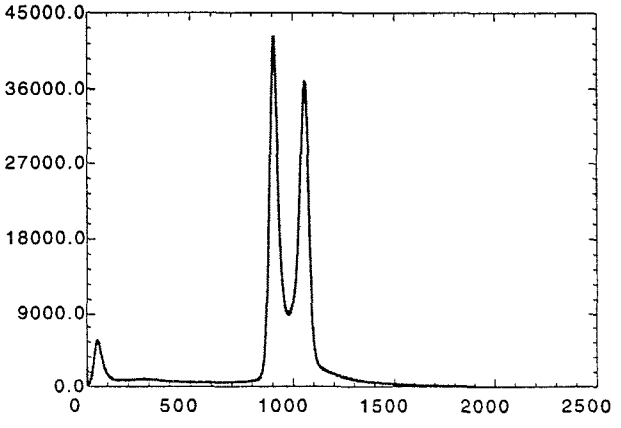

Fig.1: The histogram of a CT scan of 46 slices covering the whole colon. Each slice is 512^2 size and 5mm thick. The image density (or CT number) runs from 0 to 2454.

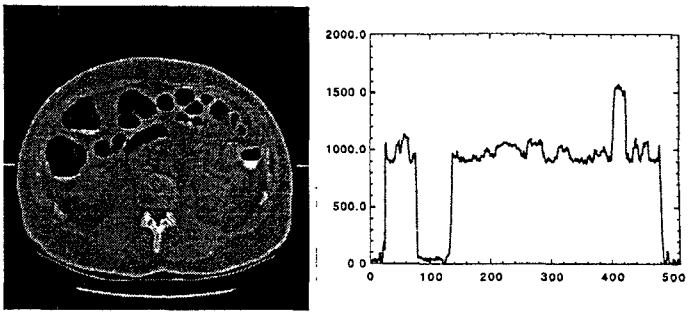

Fig.2: On the left is a slice of the 3D CT image. On the right is an one-pixel-wide horizontal profile drawn at the location shown on the slice. The enhanced fluid pixels are clearly seen.

Fig.3: On the left shows the detected body boundary and on the right is the slice image with outside-the-body voxels being stripped away.

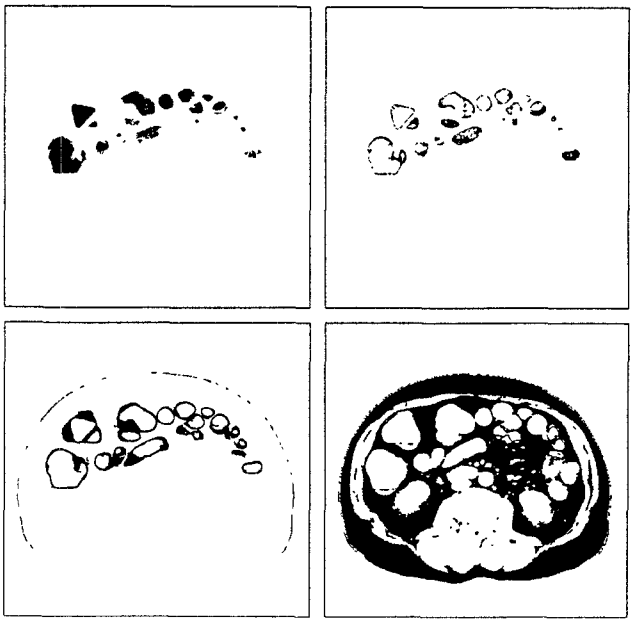

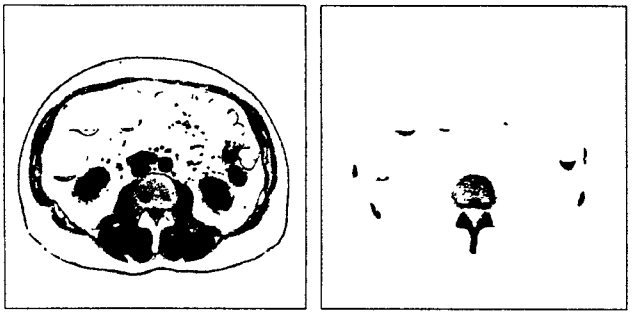

Fig.4: Segmented six classes based on the thresholds selected from the histogram. Top two segments are mostly the air voxels and the partial-volume voxels (with values close to that of the air). The middle two are mostly the partial-volume voxels (with values close to that of the soft tissue) and the soft-tissue voxels. The bottom two are mostly the muscle voxels and the bone (including enhanced fluid) voxels.

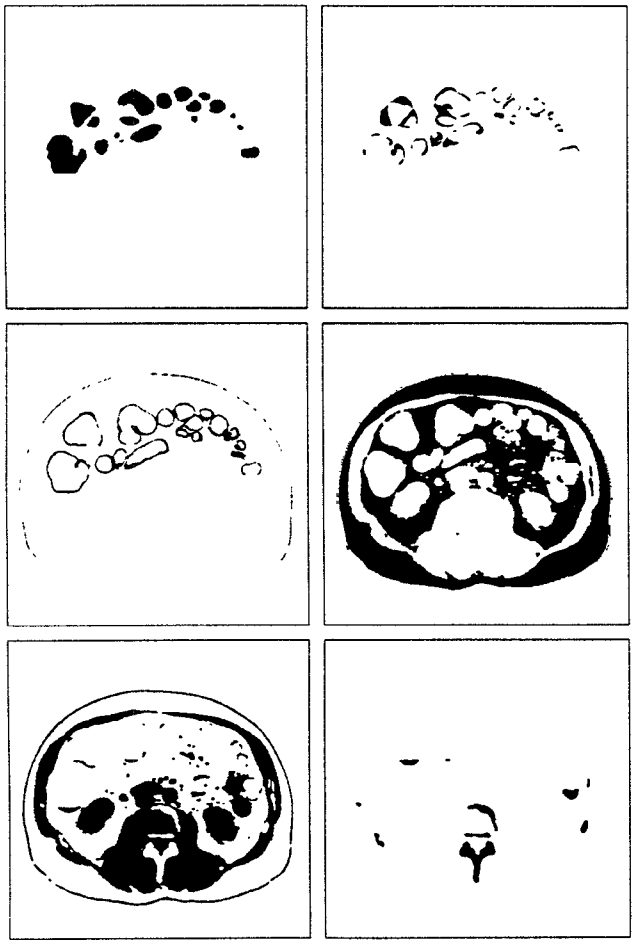

Fig.5: The segmented six classes by the MAP approach with initial estimates selected from the histogram and considering the orientation of the fluid/air boundary inside the colon.

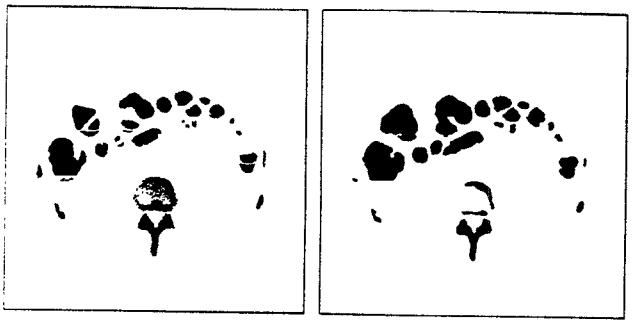

Fig.6: The summation of the three classes on the top and bottom right of Fig.4 (left) and of Fig.5 (right).

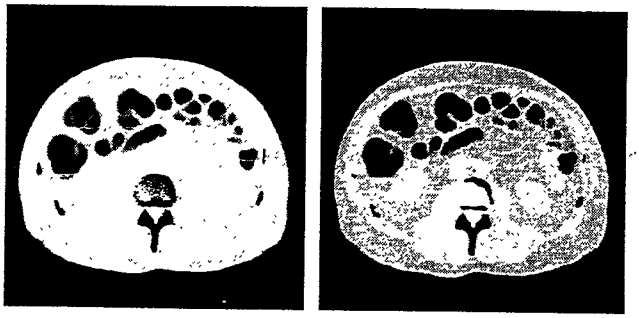

Fig.7: The slice images with colon cleansed by the threshold technique (left) and MAP approach (right).